Ocean Sci. Discuss., 12, 2231–2256, 2015
www.ocean-sci-discuss.net/12/2231/2015/
doi:10.5194/osd-12-2231-2015

Ocean Science
Discussions
Open Access

The dynamic connection of the Indonesian Throughflow, South Indian Ocean Countercurrent and the Leeuwin Current

E. Lambert, D. Le Bars, and W. P. M. de Ruijter

Institute of Marine and Atmospheric Sciences Utrecht, Utrecht University, Utrecht, the Netherlands

Received: 18 August 2015 – Accepted: 31 August 2015 – Published: 25 September 2015

Correspondence to: E. Lambert (erwin.lambert@uib.no)

Published by Copernicus Publications on behalf of the European Geosciences Union.

Abstract

East of Madagascar, wind and surface buoyancy fluxes reinforce each other, leading to frontogenesis, outcrop and an eastward along-front flow: the South Indian Ocean Countercurrent (SICC). In the east the Leeuwin Current (LC) is a unique eastern boundary current which flows poleward along Australia. It is often described as a regional coastal current forced by an off-shore meridional density gradient or a sea surface slope, yet little is known of the forcing and dynamics that control these open ocean meridional gadients. To complete this understanding, we make use of both an ocean general circulation model and a conceptual two-layer model. The SICC impinges on west Australia and adds to a sea level slope and a southward geostrophic coastal jet: the Leeuwin Current. The SICC and the LC are thus dynamically connected. An observed transport maximum of the LC around 22° S is directly related to this impingement of the SICC. The circulation of the Indonesian Throughflow (ITF) through the Indian Ocean appears to be partly trapped in the upper layer north of the outcrop line and is redirected along this outcrop line to join the eastward flow of the SICC. Shutdown of the ITF in both models strongly decreases the Leeuwin Current transport and breaks the connection between the LC and SICC. In this case, most of the SICC was found to reconnect to the internal gyre circulation in the Indian Ocean. The Indonesian Throughflow, South Indian Ocean Countercurrent and the Leeuwin Current are thus dynamically coupled.

1 Introduction

In the upper layer of the South Indian Ocean (SIO) three unique anomalous currents have been identified: the Leeuwin Current (LC, Cresswell and Golding, 1980) which flows poleward along Australia; the South Indian Ocean Counter Current (SICC, Palastanga et al., 2007) which flows from Madagascar to Australia in the upper ±300 m; and the Indonesian Throughflow (ITF, Godfrey and Golding, 1981) which flows through the

OSD
12, 2231–2256, 2015

Indonesian passages from the tropical Pacific to the Indian Ocean. The LC is unique as an eastern boundary current. Satellite altimetry observations show that this is the only eastern boundary region of enhanced mesoscale eddy activity (Schouten et al., 2005; Morrow and Birol, 1998). Across the SIO, the SICC flows against the direction of the wind (curl) driven Sverdrup circulation that moves underneath it. In contrast to other Subtropical Countercurrents (STCCs) which dissolve in the gyre, the SICC spans the full width of the basin. Large vertical shear between these opposing currents leads to (baroclinic) instability and eddies that propagate westward (Palastanga et al., 2007; Jia et al., 2011). The ITF is part of the subtropical "super gyre", a wind-driven circulation which connects the Pacific, Indian and Atlantic Oceans via the Indonesian Passages and the Agulhas and Tasman Gateways (Speich et al., 2007; de Ruijter, 1982; Ridgway and Dunn, 2007). Hypotheses on the nature and coherence of this shallow circulation system range from localized frontal jets to a system that connects the Indonesian Throughflow, the Mozambique Channel and Agulhas Current, the SICC and the Leeuwin Current System. In this study, we provide evidence supporting this latter theory of a large-scale connectivity.

Most studies of the Indian Ocean have been complementary in focusing on either the western or the eastern sector. Observations in the west have suggested the Agulhas Retroflection and Return Current as the origin of the SICC (Nauw et al., 2008). In the east, observations (Smith et al., 1991; Woo et al., 2006; Woo and Pattiaratchi, 2008; Weller et al., 2011) and Lagrangian models (Song et al., 2004; Domingues et al., 2007; Valsala and Ikeda, 2007; van Sebille et al., 2014) have identified both tropical (including ITF) and subtropical waters as a source for the LC. Basin-wide observations indicate that westward flow around 10° S (partly ITF) and eastward flow near 25° S (SICC) cross the entire basin of the Indian Ocean (see Fig. 1). These findings indicate a large-scale connectivity between the east and west. However, understanding of the dynamics and connection between these shallow currents, the LC, the SICC and the ITF, is still limited.

The Leeuwin Current is a poleward boundary current along an eastern boundary and can thus not be explained by linear theory. Early studies have pointed at observed

OSD
12, 2231–2256, 2015

meridional gradients in density and steric height as a forcing agent for the LC and the influence of the ITF in reinforcing these gradients (Godfrey and Ridgway, 1985; Weaver and Middleton, 1989). Theories on the coastal trapping of the LC have focused on vertical diffusion of Rossby waves (McCreary et al., 1986) and interaction with the continental shelf (Csanady, 1978, 1985). An ongoing program is evaluating these various proposed mechanisms (Furue et al., 2013; Benthuysen et al., 2014), but leave the problem of large-scale forcing and connectivity of the LC unanswered. To understand this large-scale forcing, one needs to understand the origin of the off-shore meridional gradients, which hints to an important role of the SICC.

The SICC shows similarities to other Subtropical Countercurrents (STCCs) which have been identified in the North Pacific (Uda and Hasunuma, 1969), South Pacific (Merle et al., 1969), North Atlantic (Reid and Mantyla, 1978) and the South Atlantic (Tsuchiya, 1985). These zonal currents have the clearest signature near 20–25° N/S in the western part of the basins. Suggested driving mechanisms are Ekman convergence (Takeuchi, 1984), isothermal convergence (Cushman-Roisin, 1984), shock formation of mixed-layer depth (de Ruijter, 1983), convergence of Rossby waves (Dewar, 1991) and mode water formation (Kobashi and Kubokawa, 2012). No single mechanism has been identified as the dominant one and all may play a part in the actual frontogenesis forming these STCCs. All studies do, however, agree that the combination of buoyancy forcing and wind stress convergence establishes the observed zonally oriented fronts with associated baroclinic frontal jets. This is accompanied by a sharp gradient of isopycnal depth (see Fig. 2) with possible outcrop along the fronts of the STCCs. The high temperatures near 10° S, sustaining the gradient, are a combined result of surface heat fluxes and the warm inflow from the Pacific: the ITF.

The Indonesian Throughflow, due to its advection of warm and fresh water, affects the hydrography in the South Indian Ocean. The effect on the circulation was first studied by Hirst and Godfrey (1993), who performed simulations using a General Circulation Model (GCM). In one run, they applied realistic bathymetry; in a second run, the Indonesian Passages were closed. In the first run allowing the ITF, a shallow south-

OSD
12, 2231–2256, 2015

eastward jet appeared near the latitude where the SICC is observed, down to the southwestern tip of Australia. In the second run, blocking of the ITF weakened this shallow circulation. They suggested that the Leeuwin Current System (LCS) is part of this shallow circulation. A model-intercomparison study of three models of varying complexity supported their conclusions (McCreary et al., 2007), yet both studies were based on coarse resolution simulations. The response of the narrow SICC and LC could therefore not be addressed. Le Bars et al. (2013) were the first to perform comparable simulations, with open and closed Indonesian Passages, using a GCM at eddy-resolving resolution. We will use these data to revise the effect of the ITF on the "realistically" simulated SICC and LC.

Three shallow currents have been identified in the South Indian Ocean: the Leeuwin Current, the South Indian Ocean Countercurrent and the Indonesian Throughflow. In this study, we aim to understand if and how these currents form a connected system. We primarily focus on the LC and the SICC and address following questions: what is the dynamic connection between the SICC and the LC? How can the general features of the shallow circulation in the SIO be understood from surface forcing? What is the role of the ITF in this system? And why are poleward eastern boundary currents like the LC not found in other basins?

To answer these questions, two models of different complexity were used. First, an ocean GCM is run at high and coarse resolution to validate against the results of Hirst and Godfrey (1993) and to show the impact of inertia on the sensitivity of the LC and SICC to the ITF. Second, a conceptual regional two-layer model is used to simulate the general shallow circulation features of the SIO from surface forcing and to reveal the sensitivity of these features to removal of the Pacific influence through the ITF. In Sect. 2, properties and configuration of both models are presented. Results of the GCM study are shown in Sect. 3 and the results of the conceptual model in Sect. 4. With both models, sensitivity of the circulation to the ITF is presented in Sect. 5, which is followed by concluding remarks in Sect. 6.

OSD
12, 2231–2256, 2015

2 Model configurations

Two models were used in this study on the dynamics of the shallow circulation in the South Indian Ocean, an ocean GCM and a conceptual two-layer model. In this section, we describe the basic properties and the configuration of both models.

2.1 General Circulation Model: Parallel Ocean Program

The Parallel Ocean Program (POP, Dukowicz and Smith, 1994) is an ocean-only general circulation model solving the primitive equations on a horizontal grid with an average resolution of 0.1° and 42 vertical layers. The atmospheric state and precipitation were taken from the CORE dataset (Large and Yeager, 2004), wind stress was computed offline using Hurrell Sea Surface Temperature climatology (Hurrell et al., 2008) and evaporation and sensible heat flux were calculated online.

For the GCM analysis, we used data from the simulations performed by Le Bars et al. (2013). After a spin-up of 75 years as described by Maltrud et al. (2010), two simulations were performed: one with realistic bathymetry; and one with closed Indonesian Passages in a similar fashion as Hirst and Godfrey (1993). Both were run for another 105 model years of which the last 50 years of simulation were averaged to approximate a steady state. Simulations were repeated on a horizontal grid with average resolution of 1.0° allowing for validation against previous modeling studies.

2.2 Conceptual model: Hallberg Isopycnal Model

The Hallberg Isopycnal Model (HIM, Hallberg, 1997, 2000) is a regional ocean-only model solving the hydrostatic primitive equations in spherical coordinates on an Arakawa C-grid. It is configured to an idealized representation of the Indian and Pacific Oceans, separated by an elongated island representing Australia (see Fig. 3). A minimum of idealized forcing terms is applied to simulate a mid-ocean eastward jet in the western basin, and a westward jet along the northern boundary of Australia with

OSD
12, 2231–2256, 2015

a predictable return pathway. These jets will be interpreted as the SICC and the ITF respectively.

To save computing time, a small eastern basin is chosen compared to the Pacific Ocean it represents. By adjusting the wind stress over this basin, we can control the transport of the simulated ITF. Over the whole domain, the bottom is flat with a depth of 1500 m below the free surface. The island is elongated to reduce effects of eddy shedding due to lateral friction at the northern and southern boundaries. Along the lateral boundaries, no-slip conditions were applied.

Because of the baroclinic structure of the South Indian Ocean circulation, where both SICC and LC have observed opposite flow in the deeper layers, we need a minimum of two layers to qualitatively describe these features. Stratification is based on Argo float data from the ARIVO project (Gaillard and Charraudeau, 2008). Average temperature and salinity above and below the 20 °C isotherm were determined for the corresponding domain and depths. To determine constant densities for the two layers, we use a linear equation of state:

$$\rho = \rho_0(1 - \alpha(T - T_0) + \beta(S - S_0)), \quad (1)$$

with $\rho_0 = 1030\,\mathrm{kg\,m^{-3}}$; $T_0 = 15\,^{\circ}\mathrm{C}$; $S_0 = 34.5\,\mathrm{psu}$; $\alpha = 1.7\times10^{-4}\ \mathrm{K^{-1}}$; and $\beta = 7.3\times10^{-4}$. This leads to two constant densities, $\rho_1 = 1029.0$ and $\rho_2 = 1031.6\,\mathrm{kg\,m^{-3}}$, for the two layers. The model was initialized with a constant interface depth of 100 m; after spinup, as described below, the interface sinks to an approximate mean depth of 200 m.

The coarse and eddy-resolving GCM simulations produce qualitatively different structures. Rather than adjusting the horizontal resolution in the two-layer model, we vary the horizontal Laplacian viscosity to distinguish between a viscous and an inertial regime.

OSD
12, 2231–2256, 2015

The internal Rossby radius constrains the horizontal resolution and dictates the horizontal viscosity:

$$R_{\text{int}} = \frac{1}{f}\sqrt{\frac{g' H_1 H_2}{H_1 + H_2}} = 22\,\text{km}. \tag{2}$$

Here, g' is the reduced gravity, $f = 10^{-4}\,\text{s}^{-1}$ is the Coriolis parameter and $H_1 = 200\,\text{m}$ and $H_2 = 1300\,\text{m}$ are the mean thicknesses of the two layers. We used a horizontal resolution of 0.2°, approximately resolving eddies. To distinguish between a viscous and an inertial regime, we applied two values for the horizontal viscosity: $A_H = 100$ and $10^4\,\text{m}^2\,\text{s}^{-1}$, giving a boundary layer scale of 17 and 79 km respectively.

The temperature structure in Fig. 2 clearly reflects the meridional gradient in surface heat flux. To simulate the effect of heating, cooling and freshwater fluxes, we applied a total buoyancy flux, following the ideas of Haney (1971). In analogy to the surface boundary condition for heating,

$$\frac{Q}{\rho_0 C_p} = K_\text{v}\frac{\partial T}{\partial z}, \tag{3a}$$

a boundary condition for buoyancy forcing can be written as

$$\frac{B\rho_0}{g} = -K_\text{v}\frac{\partial \rho}{\partial z}, \tag{3b}$$

with

$$B = \frac{g\alpha}{\rho_0 C_p} Q. \tag{3c}$$

Here, Q is the net surface heat flux in $\text{W}\,\text{m}^{-2}$; $C_p = 4181\,\text{J}\,\text{K}^{-1}\,\text{kg}^{-1}$ is the heat capacity of water; K_v is the vertical diffusivity; and B is the surface buoyancy flux in m^2s^{-3}.

OSD
12, 2231–2256, 2015

The maximum value for B of $12 \times 10^{-9} m^2 s^{-3}$ is equivalent to a surface heat flux of 31 $W m^{-2}$, a moderate value compared to estimates by Haney (1971). The applied buoyancy forcing has a constant meridional gradient and is independent on longitude (Fig. 3). The total buoyancy flux is conserved over the ocean surface.

Wind stress is applied separately over two regions. In the western basin (grey hatches in Fig. 3), a sinusoidal wind stress is applied, corrected for curvature due to the spherical coordinates. This forces a single Sverdrup gyre west of the island. In the eastern basin (black hatches in Fig. 3), a wind stress with constant curl is applied, again corrected for curvature. This pattern forces a constant northward Sverdrup transport of 15 Sv, which circulates along the northern, western and southern boundaries of the basin. The westward flow along the northern boundary represents the ITF in this model.

The combined forcing of buoyancy fluxes and wind stress can induce frontogenesis (de Ruijter, 1983; Takeuchi, 1984; Cushman-Roisin, 1984), resulting in outcrop of the interface (similar to the 20 °C isotherm in Fig. 2). South of this outcrop line, the basin becomes a one-layer system which cannot dissipate the applied buoyancy flux downward. This leads to an energy imbalance and entrainment of dense water into the upper layer. A two-layer model with outcrop can thus not reach a steady state. The timescale of this entrainment is, however, much longer than that of the spin-up. After approximately 50 model years, the total energy in the system remains nearly constant, after which it gradually increases, reflecting the entrainment process. We make a steady-state approximation at this border between the two timescales, by averaging values over the period from model year 45 to 55.

Linear theory allows for qualitative prediction of the resulting circulation, and it is instructive to do so before analysing the results. The applied wind pattern drives a depth-integrated circulation which is a combination of a Sverdrup gyre in the western basin and a jet-like circulation along the northern, western and southern boundaries, connecting to a broad constant northward flow in the eastern basin. The meridional gradient in buoyancy fluxes produces a baroclinic structure of eastward flow in the upper

OSD
12, 2231–2256, 2015

layer and westward flow in the lower layer, according to thermal wind balance:

$$\frac{\partial u}{\partial z} = \frac{g}{\rho_0 f}\frac{\partial \rho}{\partial y}. \quad (4)$$

Here, u is the zonal velocity in $\mathrm{m\,s^{-1}}$; and y and z are the meridional and vertical coordinates in m respectively. Frontogenesis can reinforce this meridional gradient, narrowing and enhancing the baroclinic structure, making the eastward flow in the upper layer more jet-like as the observed SICC.

3 GCM results

Steady state solutions of the GCM simulations with the POP model show a shallow current system in the viscous regime (Fig. 4a), resembling the findings of Hirst and Godfrey (1993). A free viscous boundary layer originates at the southwestern tip of Australia. It is to first order related to the corner shape geometry of south Australia-Tasmania, which induces a zonal "Sverdrup discontinuity" (LaCasce and Isachsen, 2007; de Ruijter, 1982). The jump in Sverdrup transport across this latitude is smoothed by the viscous free jet with westward flow south of the discontinuity and eastward north of it.

Hirst and Godfrey (1993) suggested that this circulation was connected to the LCS but could not resolve the boundary current system at their coarse resolution. Therefore, we configured the model to eddy-resolving resolution (0.1°, Fig. 4b), giving a compact poleward flowing Leeuwin Current. Both solutions show a zonal SICC east of Madagascar, fanning out broadly in the viscous case east of 90° E, while bifurcating into multiple narrow branches in the eddy-resolving case. The multi-jet structure has recently been confirmed and analysed from observations (Menezes et al., 2013).

The northern branch of the model-SICC reaches the North-West shelf, where it feeds into the coastal jet. The southern branch reaches Australia just south of the North West Cape (NWC). Cross-shore transects, taken at regular intervals of 2° along the west-Australian coast, reveal that the LC transport (see Fig. 5) upstream of the NWC (22° S,

OSD
12, 2231–2256, 2015

transect F) is low. A sharp increase is found from approximately 0.5 to 2.5 Sv just south of the NWC. This is the latitude of maximal SICC-strength and it suggests that the SICC directly connects to the LC and, in fact, largely determines its strength and existence.

The eddy-resolving simulations reproduced the main observed circulation features in the shallow Indian Ocean, including a zonal SICC and poleward flowing LC. The findings indicate a direct connection between these two currents. In order to understand the mechanism behind this connection, we will analyse the simulations of the two-layer model.

4 Conceptual model results

The two-layer model was designed to unravel and understand connectivities of currents, and their dependency on surface forcing. To visualise such connectivities in a confined basin, it is illustrative to determine a streamfunction from the simulated velocities. This is done by integrating the velocity gradients along zonal and meridional paths from each corner and averaging the resulting fields. The streamfunctions of both the viscous and the inertial simulations are shown in Fig. 6.

The viscous circulation (Fig. 6a) contains features similar to those found in the coarse GCM simulations. A mid-ocean jet departs zonally from the western boundary and connects to the southern point of the island. This jet aligns along the outcrop of the isopycnal and thus completes its circulation along the southern boundary of the upper layer. The jet obeys thermal wind balance in a two-layer system,

$$u_1 - u_2 = \frac{g'}{f}\frac{\partial h}{\partial y}, \tag{5}$$

where u_1 and u_2 are the zonal velocities (in $\mathrm{m\,s^{-1}}$) in the upper and lower layers respectively and h is the interface depth in meters. Here, h is slanted due to surface buoyancy forcing. As discussed before, frontogenesis enhances this slope $\frac{\partial h}{\partial y}$ and narrows the jet.

OSD
12, 2231–2256, 2015

To resolve the inertial regime, the simulation was repeated with a smaller lateral viscosity of $100\,m^2\,s^{-1}$. Due to rectification of the associated modes, the mid-ocean jet flows almost zonally toward the western coast of the island (Fig. 6b). Against the boundary, it sets up a pressure gradient and induces a coastally trapped poleward current, much like the observed Leeuwin Current.

To simulate a Leeuwin Current in a regional coastal model, McCreary et al. (1986) were the first to prescribe an offshore meridional gradient in surface density of approximately $3\,kg\,m^{-3}$ over a meridional extent of 2000 km. They based this value on observations, and a similar meridional density gradient is found in our eddy-resolving GCM simulations. Combining Eqs. (4) and (5), we can estimate the gradient in interface depth to produce an equivalent onshore forcing to this surface density gradient. Assuming $\frac{\partial u}{\partial z} = \frac{u_1 - u_2}{(H_1+H_2)/2}$ is the representation of velocity shear in the two-layer model, the forcing of McCreary et al. (1986) is equivalent to $\frac{\partial h}{\partial y} = 3\times10^{-4}$. This slope translates to an equatorward interface deepening of 300 m over an extent of 10°, which is indeed found. This order-of-magnitude estimation indicates that our choice of surface forcing produces an equivalent onshore forcing to drive the poleward EBC, as was prescribed by McCreary et al. (1986).

The scope of this paper is to unravel the large-scale connectivity of the shallow circulation system. We therefore refrain from discussing the detailed mechanisms of coastal trapping and frontogenesis, which have been the subject of many other studies. It is, however, noteworthy to mention that, in this model, it is most likely Ekman convergence which drives the frontogenesis leading to outcrop. This is reflected by the preferred outcrop along the zero wind stress line at 35° S.

With these simulations, we have reproduced the general features of the shallow Indian Ocean circulation system using highly idealized forcing terms. These features include a westward jet along the north of the island ("ITF"); an eastward mid-ocean jet ("SICC"); and in the inertial regime, a poleward eastern boundary current ("LC"). These three currents appear to be directly connected, as a wind-driven circulation trapped in

OSD
12, 2231–2256, 2015

the upper layer. To clarify the importance of the ITF in this system, we configured both models without the “Pacific” inflow.

5 Sensitivity to Indonesian Throughflow

Hirst and Godfrey (1993) studied the effect of the ITF by artifically closing the Indonesian Passages. This reduced the shallow eastward jet and the transport in the LCS; these results were reproduced with our GCM at coarse resolution (not shown). At eddy-resolving resolution, closure of the Indonesian Passages significantly reduces the transport through both the SICC and the LC, as can be seen in Fig. 7a. More importantly, this blocking of the ITF breaks up the connection between the modeled SICC and LC.

To analyse this sensitivity of the shallow circulation to the ITF, the wind stress over the eastern basin of the two-layer model was removed. This method is less invasive than altering the geometry, since closure of the gap north of the island would likely induce leakage from the eastern to the western basin south of the island (“Tasman leakage”). As may be expected, removal of the circulation around the island breaks up the connection between the mid-ocean jet and the poleward EBC (Fig. 7b). The combined forcing by wind and buoyancy fluxes on the western basin sustains the mid-ocean jet, which now merges into the wind-driven gyre.

Although a poleward EBC is still found along the island, this is due to a limitation of the model. Outcrop is not sustained along the southern boundary, so a baroclinic circulation is induced in the south. Such a circulation is unrealistic, because low-density waters are required south of the main outcrop line.

Both the realistic GCM and the conceptual two-layer model simulated an eastward flowing jet across the basin, which connects to a poleward EBC. Removal of the modeled ITF resulted in a weakening of the currents and breaks up the connection between the jet and the EBC, highlighting the role of the circulation around the island.

OSD
12, 2231–2256, 2015

6 Conclusions

In this study, we proposed a new mechanism for the forcing and the large-scale connections of the Leeuwin Current. It requires the circulation around Australia through the Indonesian Throughflow and the outcrop associated with the Subtropical Indian Ocean Countercurrent. This mechanism could be qualitatively described in terms of a two-layer system.

Wind stress and buoyancy forcing combine to induce frontogenesis in the South Indian Ocean, which forms a subtropical front as is identified in all subtropical oceans near 20–25° N/S. This front sets up a baroclinic system with an eastward jet in the upper layer (the Subtropical Indian Ocean Countercurrent), and a westward flow below. Moreover, this front constitutes the southern boundary of the upper layer due to outcrop of the interface between the layers.

The wind-driven circulation of the Indonesian Throughflow resides partly in this upper layer and this fraction is redirected along the subtropical front to flow zonally towards the western coast of Australia. Two regimes were identified for this connection with the Australian coast: a viscous regime, where the zonal flow bends southward towards the southwestern point of Australia, and no boundary current could be sustained; and an inertial regime, where the front crosses the Indian Ocean zonally, and the jet reaches the coast near the latitude where it departs Madagascar and feeds the Leeuwin Current. Although Ekman transport can redirect the Indonesian Throughflow directly into the Leeuwin Current, a process that accounts for the latter's relatively tropical structure, it cannot explain the forcing of the Leeuwin Current. For this, the presence of the Subtropical Indian Ocean Countercurrent is essential, demonstrating the active role of this Subtropical Countercurrent in the large-scale circulation. Without the Indonesian Throughflow, the Subtropical Indian Ocean Countercurrent would merge into the gyre like the Subtropical Countercurrents in other basins.

Whereas previous studies have focused on regional behaviour of Subtropical Countercurrents and the Leeuwin Current, we have placed these in a large-scale perspec-

OSD
12, 2231–2256, 2015

tive. Together, they form a return pathway for part of the Indonesian Throughflow into the Pacific Ocean.

Acknowledgements. Altimetry data from *MDT*_CNES-CLS13 were produced by *CLS* Space Oceanography Division and distributed by *Aviso*, with support from *Cnes* (http://www.aviso.altimetry.fr/). The authors thank Michael Kliphuis (IMAU-UU) for the support with running both models.

References

Benthuysen, J., Furue, R., McCreary, J. P., Bindoff, N. L., and Phillips, H. E.: Dynamics of the Leeuwin Current: Part 2. Impacts of mixing, friction, and advection on a buoyancy-driven eastern boundary current over a shelf, Dynam. Atmos. Oceans, 65, 39–63, doi:10.1016/j.dynatmoce.2013.10.004, 2014. 2234

Cresswell, G. and Golding, T.: Observations of a south-flowing current in the southeastern Indian Ocean, Deep-Sea Res. Pt. I, 27, 449–466, doi:10.1016/0198-0149(80)90055-2, 1980. 2232

Csanady, G. T.: The arrested topographic wave, J. Phys. Oceanogr., 8, 47–62, doi:10.1175/1520-0485(1978)008<0047:TATW>2.0.CO;2, 1978. 2234

Csanady, G. T.: "Pycnobathic" currents over the upper continental slope, J. Phys. Oceanogr., 15, 306–315, doi:10.1175/1520-0485(1985)015<0306:COTUCS>2.0.CO;2, 1985. 2234

Cushman-Roisin, B.: On the maintenance of the subtropical front and its associated countercurrent, J. Phys. Oceanogr., 14, 1179–1190, 1984. 2234, 2239

de Ruijter, W.: Asymptotic analysis of the Agulhas and Brazil current systems, J. Phys. Oceanogr., 12, 361–373, doi:10.1175/1520-0485(1982)012<0361:AAOTAA>2.0.CO;2, 1982. 2233, 2240

de Ruijter, W. P. M.: Frontogenesis in an advective mixed-layer model, J. Phys. Oceanogr., 13, 487–495, 1983. 2234, 2239

Dewar, W. K.: Arrested fronts, J. Mar. Res., 49, 21–52, doi:10.1357/002224091784968576, 1991. 2234

Domingues, C. M., Maltrud, M. E., Wijffels, S. E., Church, J. A., and Tomczak, M.: Simulated Lagrangian pathways between the Leeuwin Current System and the upper-

OSD
12, 2231–2256, 2015

ocean circulation of the southeast Indian Ocean, Deep-Sea Res. Pt. II, 54, 797–817, doi:10.1016/j.dsr2.2006.10.003, 2007. 2233

Dukowicz, J. K. and Smith, R. D.: Implicit free-surface method for the Bryan-Cox-Semtner ocean model, J. Geophys. Res., 99, 7991–8014, doi:10.1029/93JC03455, 1994. 2236

Furue, R., McCreary, J. P., Benthuysen, J., Phillips, H. E., and Bindoff, N. L.: Dynamics of the Leeuwin Current: Part 1. Coastal flows in an inviscid, variable-density, layer model, Dynam. Atmos. Oceans, 63, 24–59, doi:10.1016/j.dynatmoce.2013.03.003, 2013. 2234

Gaillard, F. and Charraudeau, R.: New climatology and statistics over the global ocean, Mersea Project Rep. CNRS-STR-001 Del 5.4.7, 26 pp., 2008. 2237, 2251

Godfrey, J. S. and Golding, T.: The Sverdrup relation in the Indian Ocean, and the effect of Pacific-Indian Ocean Throughflow on Indian Ocean Circulation and on the East Australian Current, J. Phys. Oceanogr., 11, 771–779, 1981. 2232

Godfrey, J. S. and Ridgway, K. R.: The large-scale environment of the poleward-flowing Leeuwin Current, Western Australia: longshore steric height gradients, wind stresses and geostrophic flow, J. Phys. Oceanogr., 15, 481–495, doi:10.1175/1520-0485(1985)015<0481:TLSEOT>2.0.CO;2, 1985. 2234

Hallberg, R.: Time integration of diapycnal diffusion and Richardson Number – dependent mixing in isopycnal coordinate ocean models, Mon. Weather Rev., 128, 1402–1419, doi:10.1175/1520-0493(2000)128<1402:TIODDA>2.0.CO;2, 2000. 2236

Hallberg, R. W.: HIM: The Hallberg Isopycnal Coordinate Primitive Equation Model, NOAA Geophysical Fluid Dynamics Laboratory Tech. Report, available at: https://www.gfdl.noaa.gov/cms-filesystem-action/user_files/rwh/him_description.pdf (last access: 24 September 2015), 1997. 2236

Haney, R. L.: Surface thermal boundary condition for ocean circulation models, J. Phys. Oceanogr., 1, 241–248, doi:10.1175/1520-0485(1971)001<0241:STBCFO>2.0.CO;2, 1971. 2238, 2239

Hirst, A. C. and Godfrey, J. S.: The role of Indonesian Throughflow in a global ocean GCM, J. Phys. Oceanogr., 23, 1057–1086, doi:10.1175/1520-0485(1994)024<1895:TRTASC>2.0.CO;2, 1993. 2234, 2235, 2236, 2240, 2243

Hurrell, J. W., Hack, J. J., Shea, D., Caron, J. M., and Rosinski, J.: A new sea surface temperature and sea ice boundary dataset for the community atmosphere model, J. Climate, 21, 5145–5153, doi:10.1175/2008JCLI2292.1, 2008. 2236

OSD
12, 2231–2256, 2015

Jia, F., Wu, L., and Qiu, B.: Seasonal modulation of Eddy kinetic energy and its formation mechanism in the Southeast Indian Ocean, J. Phys. Oceanogr., 41, 657–665, doi:10.1175/2010JPO4436.1, 2011. 2233

Kobashi, F. and Kubokawa, A.: Review on North Pacific Subtropical Countercurrents and Subtropical Fronts: role of mode waters in ocean circulation and climate, J. Oceanogr., 68, 21–43, doi:10.1007/s10872-011-0083-7, 2012. 2234

LaCasce, J. H. and Isachsen, P. E.: On sverdrup discontinuities and vortices in the Southwest Indian Ocean, J. Phys. Oceanogr., 37, 2940–2950, doi:10.1175/2007JPO3652.1, 2007. 2240

Large, W. G. and Yeager, S. G.: Diurnal to decadal global forcing for ocean and sea–ice models: {the} data sets and flux climatologies., NCAR Tech. Note, TN-460+ST, 105 pp., doi:10.5065/D6KK98Q6, 2004. 2236

Le Bars, D., Dijkstra, H. A., and De Ruijter, W. P. M.: Impact of the Indonesian Throughflow on Agulhas leakage, Ocean Sci., 9, 773–785, doi:10.5194/os-9-773-2013, 2013. 2235, 2236

Maltrud, M., Bryan, F., and Peacock, S.: Boundary impulse response functions in a century-long eddying global ocean simulation, Environ. Fluid Mech., 10, 275–295, doi:10.1007/s10652-009-9154-3, 2010. 2236

McCreary, J. P., Shetye, S. R., and Kundu, P. K.: Thermohaline forcing of eastern boundary currents: With application to the circulation off the west coast of Australia, J. Mar. Res., 44, 71–92, doi:10.1357/002224086788460184, 1986. 2234, 2242

McCreary, J. P., Miyama, T., Furue, R., Jensen, T., Kang, H. W., Bang, B., and Qu, T.: Interactions between the Indonesian Throughflow and circulations in the Indian and Pacific Oceans, Prog. Oceanogr., 75, 70–114, doi:10.1016/j.pocean.2007.05.004, 2007. 2235

Menezes, V. V., Phillips, H. E., Schiller, A., Domingues, C. M., and Bindoff, N. L.: Salinity dominance on the Indian Ocean Eastern Gyral current, Geophys. Res. Lett., 40, 5716–5721, doi:10.1002/2013GL057887, 2013. 2240

Merle, J., Rotschi, H., and Voituriez, B.: Zonal circulation in the Tropical Western South Pacific at 170 E, Bull. Jpn. Soc. Fish., 91–98, 1969. 2234

Morrow, R. and Birol, F.: Variability in the southeast Indian Ocean from altimetry: forcing mechanisms for the Leeuwin Current, J. Geophys. Res.-Oceans, 103, 18529–18544, doi:10.1029/98JC00783, 1998. 2233

Nauw, J. J., van Aken, H. M., Webb, A., Lutjeharms, J. R. E., and de Ruijter, W. P. M.: Observations of the southern East Madagascar Current and undercurrent and countercurrent system, J. Geophys. Res.-Oceans, 113, 1–15, doi:10.1029/2007JC004639, 2008. 2233

OSD
12, 2231–2256, 2015

Palastanga, V., van Leeuwen, P. J., Schouten, M. W., and de Ruijter, W. P. M.: Flow structure and variability in the subtropical Indian Ocean: Instability of the South Indian Ocean countercurrent, J. Geophys. Res.-Oceans, 112, 1–11, doi:10.1029/2005JC003395, 2007. 2232, 2233

Reid, J. L. and Mantyla, A. W.: On the mid-depth circulation of the North Pacific Ocean, J. Phys. Oceanogr., 8, 946–951, doi:10.1175/1520-0485(1978)008<0946:OTMDCO>2.0.CO;2, 1978. 2234

Ridgway, K. R. and Dunn, J. R.: Observational evidence for a Southern Hemisphere oceanic supergyre, Geophys. Res. Lett., 34, 1–5, doi:10.1029/2007GL030392, 2007. 2233

Schouten, M. W., de Ruijter, W. P. M., and Ridderinkhof, H.: A seasonal intrusion of subtropical water in the Mozambique Channel, Geophys. Res. Lett., 32, 1–4, doi:10.1029/2005GL023131, 2005. 2233

Smith, R. L., Huyer, A., Godfrey, J. S., and Church, J. A.: The Leeuwin Current off Western Australia, 1986–1987, J. Phys. Oceanogr., 21, 323–345, doi:10.1175/1520-0485(1991)021<0323:TLCOWA>2.0.CO;2, 1991. 2233

Song, Q., Gordon, A. L., and Visbeck, M.: Spreading of the Indonesian Throughflow in the Indian Ocean, J. Phys. Oceanogr., 34, 772–792, doi:10.1175/1520-0485(2004)034<0772:SOTITI>2.0.CO;2, 2004. 2233

Speich, S., Blanke, B., and Cai, W.: Atlantic meridional overturning circulation and the Southern Hemisphere supergyre, Geophys. Res. Lett., 34, 1–5, doi:10.1029/2007GL031583, 2007. 2233

Takeuchi, K.: Numerical study of the Subtropical Front and the Subtropical Countercurrent, Journal of the Oceanographical Society of Japan, 40, 371–381, 1984. 2234, 2239

Tsuchiya, M.: Evidence of a double-cell subtropical gyre in the South Atlantic Ocean, J. Mar. Res., 43, 57–65, doi:10.1357/002224085788437271, 1985. 2234

Uda, M. and Hasunuma, K.: The eastward subtropical countercurrent in the Western North Pacific Ocean, Journal of the Oceanographical Society of Japan, 25, 201–210, 1969. 2234

Valsala, V. K. and Ikeda, M.: Pathways and effects of the Indonesian Throughflow water in the Indian Ocean using particle trajectory and tracers in an OGCM, J. Climate, 20, 2994–3017, doi:10.1175/JCLI4167.1, 2007. 2233

van Sebille, E., Sprintall, J., Schwarzkopf, F. U., Gupta, A. S., Santoso, A., England, M. H., Biastoch, A., and Böning, C. W.: Pacific-to-Indian Ocean connectivity: Tasman leakage, In-

OSD
12, 2231–2256, 2015

donesian Throughflow, and the role of ENSO, J. Geophys. Res.-Oceans, 119, 1365–1382, doi:10.1002/2013JC009525, 2014. 2233

Weaver, A. J. and Middleton, J. H.: On the dynamics of the Leeuwin Current, J. Phys. Oceanogr., 19, 626–648, doi:10.1175/1520-0485(1989)019<0626:OTDOTL>2.0.CO;2, 1989. 2234

Weller, E., Holliday, D., Feng, M., Beckley, L., and Thompson, P.: A continental shelf scale examination of the Leeuwin Current off Western Australia during the austral autumn-winter, Cont. Shelf. Res., 31, 1858–1868, doi:10.1016/j.csr.2011.08.008, 2011. 2233

Woo, M. and Pattiaratchi, C.: Hydrography and water masses off the western Australian coast, Deep-Sea Res. Pt. I, 55, 1090–1104, doi:10.1016/j.dsr.2008.05.005, 2008. 2233

Woo, M., Pattiaratchi, C., and Schroeder, W.: Dynamics of the Ningaloo Current off Point Cloates, Western Australia, Mar. Freshwater Res., 57, 291–301, doi:10.1071/MF05106, 2006. 2233

OSD

12, 2231–2256, 2015

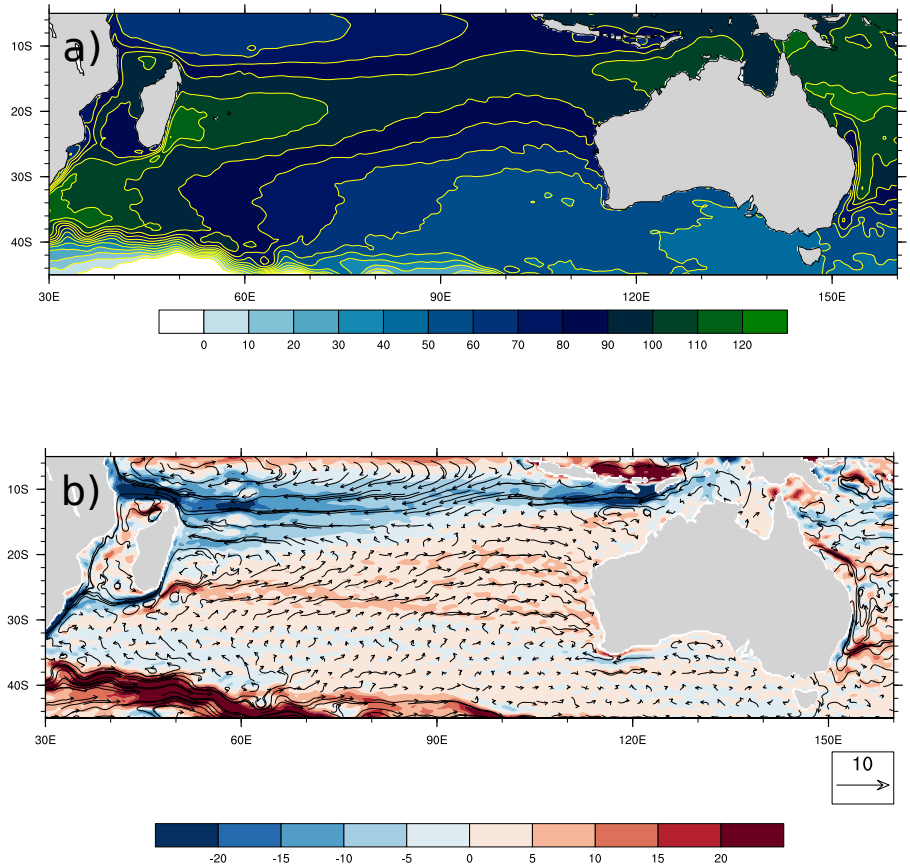

Figure 1. (a) Mean dynamic topography (cm) from altimetry product *MDT*_CNES-CLS13. **(b)** Derived geostrophic velocities (cm s^{-1}), where positive values indicate an eastward component.

OSD
12, 2231–2256, 2015

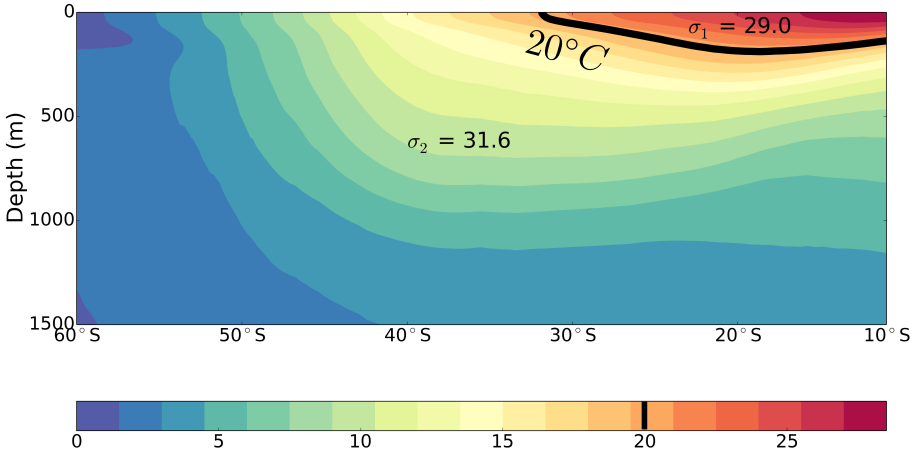

Figure 2. Meridional section of temperature (°C) at 80° E from Argo floats (ARIVO project, Gaillard and Charraudeau, 2008). The 20 °C isotherm is used to divide the basin into an upper and lower layer. For both layers, average relative densities σ are denoted, which are used for defining the stratification of the two-layer model. The isotherm shows outcrop near 30° S, marking the southern boundary of the upper layer.

OSD
12, 2231–2256, 2015

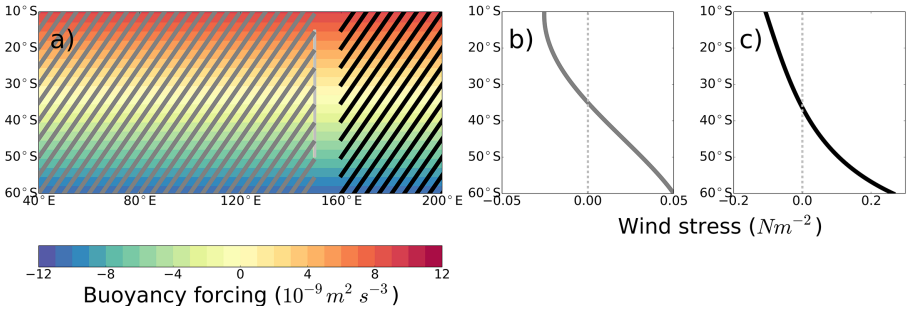

Figure 3. Configuration of the conceptual two-layer model. **(a)** Model domain, applied buoyancy forcing (shading) and two areas where wind stress is applied (hatches). The light grey area at 150° E indicates the elongated island. **(b)** Wind stress simulating a gyre (grey) and **(c)** ITF (black) applied to respective areas as indicated in panel **(a)**.

OSD
12, 2231–2256, 2015

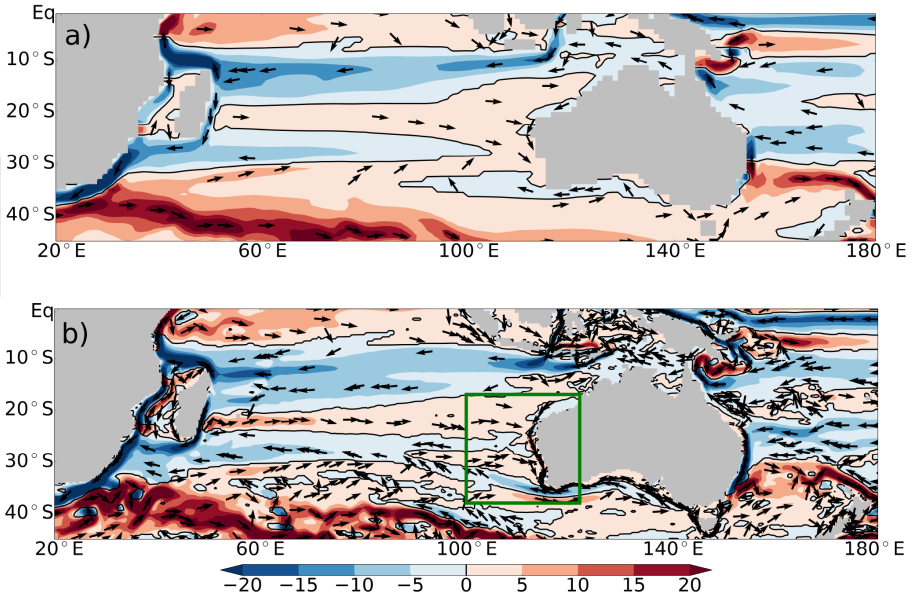

Figure 4. Steady-state horizontal velocities averaged over the top 200 m ($cm\,s^{-1}$) from the GCM simulations. **(a)** Coarse resolution (1.0°), **(b)** eddy-resolving resolution (0.1°). Positive values indicate an eastward component. Unit vectors are added at local maxima to show the direction of the flow. The green box indicates the area shown in Fig. 5a.

OSD
12, 2231–2256, 2015

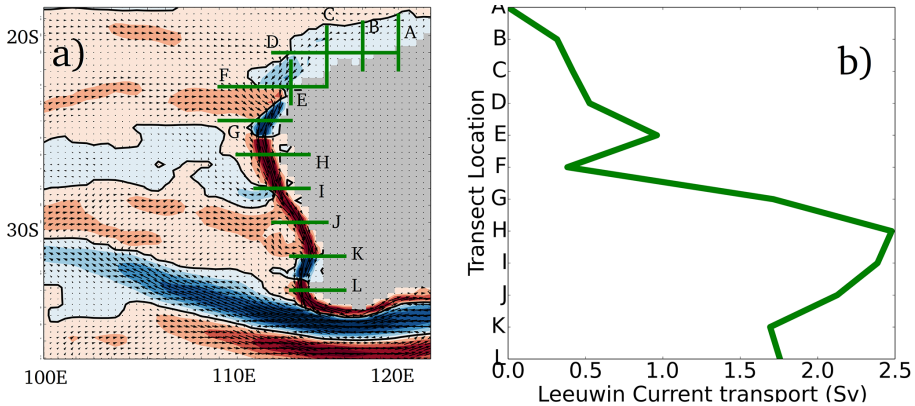

Figure 5. (a) Inlet from Fig. 4 with indicated transects along the western coast. Transects are taken at intervals of 2° along the coast. Labels A-L are ordered from up- to downstream where A, B, C and E are meridional sections, the others zonal. **(b)** Cross-transect velocities are integrated down to the depth of zero velocity to give an LC transport. This depth increases monotonically from 150 m at transect A to 300 m at transect L. Transect F marks the latitude of the North West Cape: 22° S.

OSD
12, 2231–2256, 2015

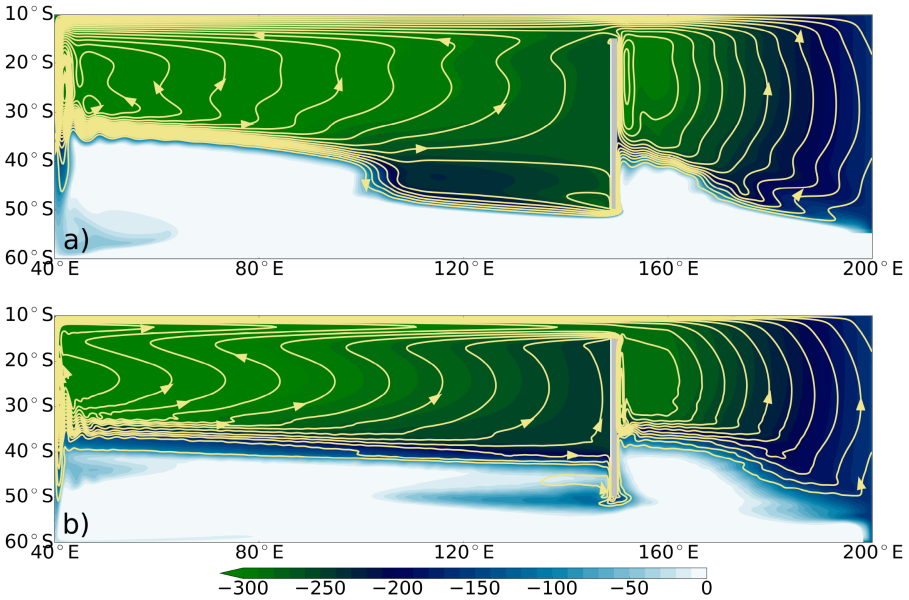

Figure 6. Streamfunction (yellow contours, interval 1 Sv) of **(a)** viscous and **(b)** inertial circulation in the upper layer as forced by the configuration shown in Fig. 3. Colour shading indicates the depth of the interface relative to the free surface in meters. The white areas thus represent areas of (near-)outcrop.

OSD
12, 2231–2256, 2015

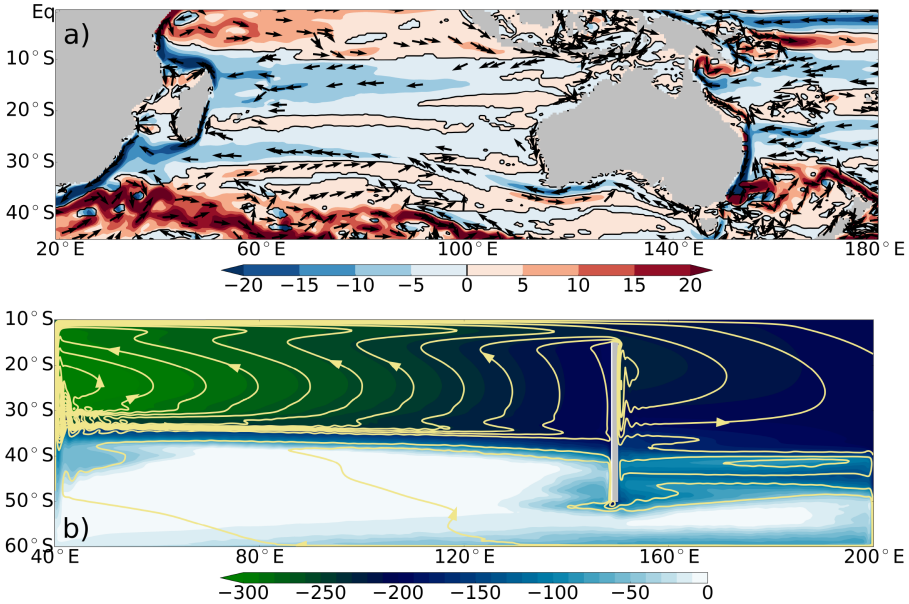

Figure 7. (a) As Fig. 4 with closed Indonesian Passages. **(b)** As Fig. 6 without the wind forcing in the eastern basin (black hatches in Fig. 3).

OSD
12, 2231–2256, 2015